I. Engineering Property Prediction Tools for Tailored Polymer Composite Structures

Principal Investigator: Ba Nghiep Nguyen
Pacific Northwest National Laboratory (PNNL)
902 Battelle Boulevard, P.O. Box 999, MS: K5-22, Richland, WA 99354
(509) 375 3634; Fax: 509-375 673; e-mail: Ba.Nguyen@pnl.gov

Principal Investigator: James D Holbery
PNNL
902 Battelle Boulevard – P.O. Box 999 – MS: K5-22, Richland, WA 99354
(509) 375 3686; Fax: 509-375 6736; e-mail: James.Holbery@pnl.gov

Principal Investigator: Vlastimil Kunc
Oak Ridge National Laboratory (ORNL)
P.O. Box 2009, Oak Ridge, TN 37831
(865) 574 8010; Fax: 865-574-0740; e-mail: kuncv@ornl.gov

Technology Area Development Manager: Joseph A. Carpenter
(202) 586-1022; fax: (202) 586-1600; e-mail: joseph.carpenter@ee.doe.gov

Expert Technical Monitor: Philip S. Sklad
(865) 574-5069; fax: (865) 576-4963; e-mail: skladps@ornl.gov

---

Contractors: Pacific Northwest National Laboratory, Oak Ridge National Laboratory
Contract No.: DE-AC06-76RL01830, DE-AC05-00OR22725

Objective

- Enable the optimum design of lightweight automotive structural components using injection- molded long-fiber-reinforced thermoplastic (LFT) composites.

Approach

Phase I: Technical feasibility assessment

- Perform a technical assessment of current process models and computational methods for short-fiber polymer injection-molded composites in order to determine their accuracy, limitations and potential applications to LFTs.
- Identify the research directions needed to develop process and constitutive models for LFTs.
- Understand and examine the LFT emerging microstructure, characterization techniques and material processing.
- Characterize fiber orientation in LFT samples.
- Examine the molding behavior of glass and carbon fibers.

Phase II: Research and development

Develop an integrated approach that links process to structural modeling allowing the optimum design of LFT composite structures. This work includes:

- development of process models for LFTs that allow simulations of LFT structures in order to predict flow-induced fiber orientation and other microstructural features,
- development and implementation of LFT constitutive models for structural finite-element analyses that make use of the composite microstructure predicted by process modeling. These constitutive models will predict the composite thermoelastic properties and its nonlinear behaviors due to damage, fatigue, creep and impact,
- development of characterization methods for LFT materials,
- injection-molding of larger samples and complex geometries,
- experimental testing to determine the model parameters and to validate the process and constitutive models.

Accomplishments

- Long-fiber materials have been specified and procured from MTI Thermoplastics with either glass fibers (GF) or carbon fibers (CF) in a polypropylene (PP) matrix. The materials include 40% by weight GF in a PP matrix (i.e., 40%GF/PP), 31%CF/PP, and 31%Ni-Coated CF/PP. These weight percents give a common volume fraction of approximately 20%.
- In conjunction with Delphi Automotive, parts have been injection molded in three geometries under specific test conditions. These samples, molded from both CF/PP and GF/PP materials, were subsequently analyzed for both fiber orientation and mechanical properties.
- A technical assessment of the current process models for discontinuous fiber composites was conducted that provided insight on their limitations and applicability to LFTs.
- Numerical simulations of LFT injection molded samples were carried out using the current models to predict the fiber orientations. The predicted orientations were compared with the experimental data to assess the accuracy of the current models applied to LFTs.
- Computational models have been developed to predict the thermoelastic properties of LFTs. These models account for fiber length and orientation distribution in addition to the constituents' thermoelastic properties.
- A comprehensive website was developed to collect all data, publications, and updates for the program participants.
- Experimental methods for measuring fiber orientation and fiber length in LFTs were evaluated.
- Fiber orientation was evaluated for a set of specimens using a University of Leeds (Leeds) system.
- Measurements from Leeds system were validated via manual measurement.
- Fiber-length measurement techniques for glass and carbon fibers were developed.
- Method for separation of long carbon fibers was developed.
- Mechanical tests were performed to assess mechanical properties of LFT samples.

Future Direction

- Develop a material characterization matrix to obtain composite constitutive parameters for model input
- Develop process and property prediction models for LFTs
- Further develop non-destructive techniques to determine fiber orientation, fiber length, and fiber attrition in molded parts
- Procure materials and subsequently mold test samples with selected Tier 1 molder
- Develop orientation models for implementation in the Moldflow software for improved simulation of LFT composites.

Introduction

Recently, injection-molded long-fiber thermoplastics (LFTs) have generated great interest within the automotive industry as these materials can be used for structural applications in order to reduce vehicle weight. However, injection-molding of these materials poses a great challenge because of two main reasons: (i) no process models for LFTs have been developed that can be used to predict the processing of an LFT part, and (ii) no experimental characterization methods exist to fully characterize the as-formed LFT microstructure to determine the fiber orientation and length distributions and fiber dispersion that are critical for any process model development.

This report summarizes the work conducted during fiscal year (FY) 2006 that includes (i) the assessment of current process modeling approaches, (ii) experimental evaluation of LFT microstructure and mechanical properties, and (iii) the computation of thermoelastic properties using the measured and predicted orientation distributions as well as the measured fiber-length distribution. Our objective is two-fold. First, it is necessary to assess current process models and characterization techniques in order to determine their capabilities and limitations, and the necessary developments for LFTs. Second, before modeling the nonlinear behaviors of LFTs, it is essential to develop computation tools for predicting the elastic and thermoelastic properties of these materials.

Assessment of Current Process Modeling Approaches

During FY 2006, we assessed process models for fiber-reinforced injection-molded thermoplastics in order to determine the limitations and applicability of these models to predict the as-formed composite microstructure. The details of this study are presented in [1-2]. First, the concentration regimes were examined to facilitate the understanding of different types of fiber-fiber interaction that can occur for a given fiber volume fraction. Basically, there are three concentration regimes which are the dilute, semi-concentrated (or semi-dilute), and concentrated regimes [3].

After the formulation of the fiber suspension flow problem and the simplification leading to the Hele-Shaw approach, the interaction mechanisms were examined. In general, fiber-fiber interactions can be classified into two categories: *hydrodynamic interaction* [4] and *mechanical interaction* [5]. Hydrodynamic interactions are hydrodynamic in nature and include *short-* and *long-range interactions* [4, 6]. The long-range hydrodynamic interaction results as a fiber is placed in the disturbance flow field of other fibers. The short-range hydrodynamic interaction is due to the lubrication forces and torques. At high concentrations, mechanical interactions due to direct fiber-fiber contacts and Coulomb friction occur [7-8].

Depending on the concentration regimes, both hydrodynamic and mechanical interactions do occur in injection-molded short-fiber-reinforced thermoplastic (SFT) and LFT systems. For SFTs, Folgar and Tucker [9] added a diffusion term to the Jeffrey's dilute solution in order to represent the randomizing effect of the fiber-fiber interaction in concentrated suspensions. This term hence depicts the hydrodynamic interactions. Later, Advani and Tucker [10] recast the Folgar-Tucker equation in terms of the fiber orientation tensor components as:

$$\frac{DA_{ij}}{Dt} + \frac{1}{2}(\omega_{ik}A_{kj} - A_{ik}\omega_{kj}) = \frac{1}{2}\kappa(\dot{\gamma}_{ik}A_{kj} + A_{ik}\dot{\gamma}_{kj} - 2\dot{\gamma}_{kl}A_{ijkl}) + 2C_I\dot{\gamma}(\delta_{ij} - 3A_{ij}) \quad (1)$$

where A_{ij}, A_{ik}, and A_{kj} are the components of the second-order orientation tensor, and A_{ijkl} is the fourth-order orientation tensor. δ_{ij} is the identity tensor, and ω_{ik} and ω_{kj} are the components of the vorticity tensor. $\dot{\gamma}_{ik}$, $\dot{\gamma}_{kj}$, and $\dot{\gamma}_{kl}$ are the components of the rate of the deformation tensor whose scalar magnitude is $\dot{\gamma}$. κ and C_I are material constants; κ depends on the fiber aspect ratio *r*, and C_I is called the interaction coefficient. If $C_I = 0$ and, $\kappa = (r^2 - 1)/(r^2 + 1)$, Eq. (1) is then Jeffrey's equation for the motion of a rigid ellipsoidal shape fiber in a Newtonian solvent. This

is strictly valid for dilute suspensions in which the fiber-fiber interaction is absent or negligible.

Recent experience with SFTs suggests that the rate of orientation in concentrated fiber suspensions is slower than the standard model prediction (Eq. (1)), and thus the *SRF* (strain reduction factor) factor has been introduced to improve the agreement between prediction and experiment [11-12]:

$$\frac{DA_{ij}}{Dt} + \frac{1}{2\,SRF}(\omega_{ik}A_{kj} - A_{ik}\omega_{kj}) = \frac{1}{SRF}[\frac{1}{2}\kappa(\dot{\gamma}_{ik}A_{kj} + A_{ik}\dot{\gamma}_{kj} - 2\dot{\gamma}_{kl}A_{ijkl}) + 2C_I\dot{\gamma}(\delta_{ij} - 3A_{ij})] \quad (2)$$

One problem arises in Eq. (2) if $SRF \neq 1$, namely it does not necessarily give the same answer in every coordinate system. To overcome this issue, in this report, a new model, called the *reduced strain closure RSC* model, was used that can be applied to all flows and coordinate systems. Next, the establishment of the rheological constitutive equation was studied. A constitutive relation is necessary to relate the stress in the suspension to the rate of deformation, the fiber orientation state and the suspension parameters such as the fiber volume fraction, the fiber aspect ratio, and the viscosity of the suspending liquid. As the compressibility of the suspending liquid and the fibers are negligible, the total stress σ_{ij} is separated into an hydrostatic contribution from the pressure *P* plus a contribution from the suspension defined as the *extra stress*, τ_{ij} [3]:

$$\sigma_{ij} = -P\delta_{ij} + \tau_{ij} \quad (3)$$

where

$$\tau_{ij} = 2\eta(\dot{\gamma},T)\dot{\gamma}_{ij} + 2\eta(\dot{\gamma},T)N_p A_{ijkl}\dot{\gamma}_{kl} \quad (4)$$

$\eta(\dot{\gamma},T)$ is the suspension viscosity which is in general a function of the strain rate and temperature *T*. N_P is defined as the particle number and is a dimensionless parameter dependent on the fiber volume fraction and aspect ratio. If N_P is equal to zero, Eq. (4) is the constitutive relation of a generalized Newtonian fluid in which the stress field is assumed not to be dependent on the orientation state. This is the assumption for using a decoupled flow/orientation approach.

The coupled and decoupled flow/orientation approach was also reviewed. In a decoupled approach, the fluid-flow problem is first solved as if the fibers were not present, and the resulting kinematics (i.e., velocity field) is used to compute the fiber orientation. On the other hand, in a coupled problem the flow and orientation equations must be solved simultaneously. To date, the coupled approach has not been implemented in commercial finite-element software packages.

This section applies the current capabilities to computationally predict fiber orientation for three different LFT materials, using two different mold geometries: an *end-gated strip* and a *center-gated disk*. In order to compute the orientation state for an injection-molding operation, the equations of balance of mass, momentum, and energy must be solved so that a velocity field can be computed. A program named ORIENT was used to solve the velocity profile and the orientation in the above-mentioned geometries [11]. ORIENT uses the Hele-Shaw approximation for solving for the velocity field in mold-filling operations where the velocity solution is decoupled from the orientation solution.

Table 1 provides a concise summary of each of the samples molded. The sample code identifies each material as "PNNLwxyz." The letter "w" identifies each material; "x" indicates either fast or slow injection speeds; y corresponds to the sample thickness in mm (all samples with orientation measurements were 3 mm thick); and z indicates the part geometry (D or I, indicating a disk or ISO plaque). Material A has a polypropylene matrix with a 40% weight fraction of glass fibers. Material B is a polypropylene matrix with 31% weight fraction of carbon fibers, and material C is the same as material B, with the exception that the carbon fibers are nickel-coated. The center-gated disk is 177.8 mm in diameter, while the ISO plaque is 90 mm long and 80 mm wide. Moldflow, Inc (Ithaca, NY) performed a complete evaluation of materials A and C and supplied the appropriate rheological and thermal properties.

Table 1. Summary of materials, injection speed, and mold geometry for each of the studied samples.

Sample Code	Material	Injection Speed Setting		Geometry
		Fill Speed	Fill Time [s]	
PNNLAF3D	A	Fast	0.65	Disk
PNNLAS3D	A	Slow	4.79-4.18	Disk
PNNLAF3I	A	Fast	0.48	ISO Plaque
PNNLAS3I	A	Slow	3.33	ISO Plaque
PNNLBF3D	B	Fast	0.67-0.81	Disk
PNNLBS3D	B	Slow	4.93-4.96	Disk
PNNLCF3D	C	Fast	0.67	Disk
PNNLCS3D	C	Slow	4.99-5.01	Disk
PNNLCF3I	C	Fast	0.475-0.480	ISO Plaque
PNNLCS3I	C	Slow	3.69-3.73	ISO Plaque

The properties of material B were assumed to be equivalent to those of material C. In order to compare the predicted and measured orientations, each of the samples presented in Table 1 were analyzed at three regions denoted A, B, and C. For the ISO plaques, region A was centered near the inlet at x = 15 mm, region B was centered approximately half-way down the length of the plaque at x = 45 mm, and region C was closer to the end of the plaque, centered at x = 75 mm. Each of the regions was located centrally in the cross-flow direction. For the center-gated disk, region A was located near the inlet at r = 6 mm, region B was at r = 34 mm, and region C was closer to the edge of the disk at r = 64 mm, where r is the radius of the disk. Each of the samples was 3 mm thick.

Orientation measurements were preformed by ORNL staff at GM using a Leeds image analysis system developed by Hine et al. [12]. The important orientation descriptors are the orientation tensor elements A_{11}, A_{22}, A_{33}, and A_{31}. A_{11}, A_{22}, and A_{33} range between 0 and 1. Figures 1-4 illustrate the orientation tensor components at region B for some of the selected samples.

Experimental Evaluation of LFT Microstructure and Mechanical Properties

The experimental effort was focused on development and validation of procedures for fiber-orientation and fiber-length measurements and on providing measurements of these quantities in molded samples at specific locations. Thermo-elastic properties were measured at identical locations to allow correlation of mechanical properties to local material microstructure.

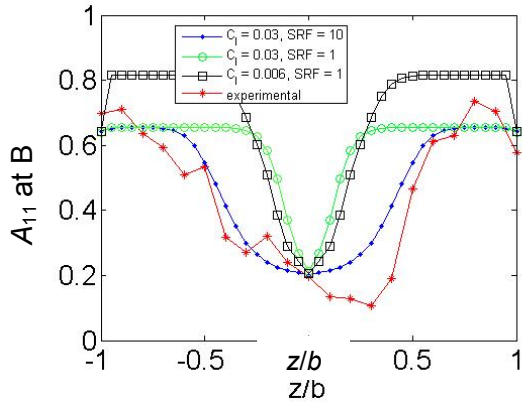

Figure 1. A_{11} vs. non-dimensional thickness coordinate z/b for PNNLAF3I.

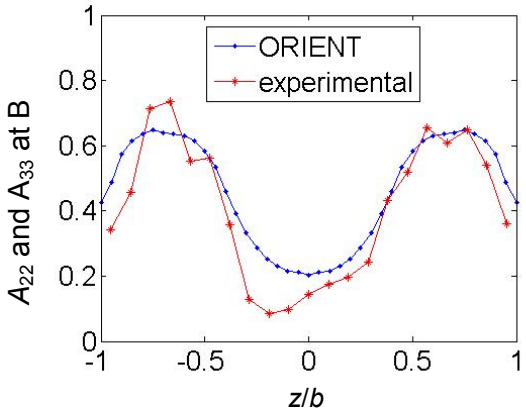

Figure 2. A_{11} vs. non-dimensional thickness coordinate z/b for PNNLAS3I at region B. SRF = 30 and C_I = 0.03.

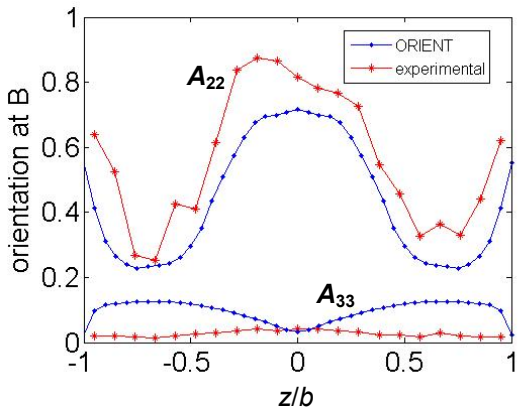

Figure 3. A_{22} and A_{33} vs. non-dimensional thickness coordinate *z/b* for PNNLAS3I at region B. *SRF* = 30 and C_I = 0.03.

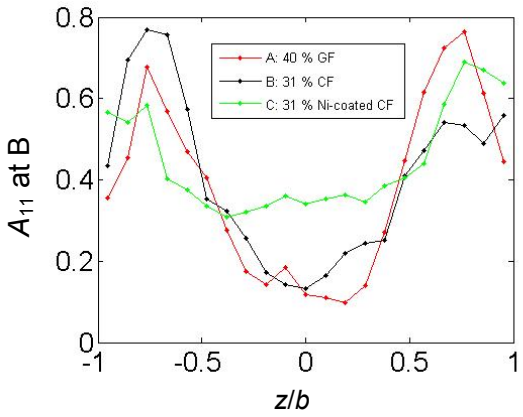

Figure 4. Experimental A_{11} vs. *z/b* at region B for all three materials. The samples were slow-filled disks.

For fiber-orientation measurements, tensile, ISO and disk samples were sectioned. Specimens were mounted in a resin and polished. Glass specimens were etched and sputter coated with gold to increase contrast between fibers and matrix.

Polished samples were analyzed using an optical system developed by University of Leeds. This system collects an array of digital images from a cross-section of a sample and performs assembly of these images. Fibers are assumed to be straight cylinders, therefore, the cross-sections of fibers in a given plane should be visible as ellipses. The Leeds system distinguishes fibers from matrix through thresholding and ellipses are fitted to the thresholded image. Fiber orientation is determined based on the ratio and size of minor and major axes of ellipses fitted to the image. Leeds analysis was performed in three locations on all specimens, with the exception of 6-mm-thick ISO bars. Voids in these samples prevented meaningful analysis.

The system assumes that fibers are straight and that ellipses can be fitted to a cross-section of each fiber crossing the plane. These long fibers were not counted in the Leeds analysis, therefore raising the question about the accuracy of the measurement. Discounting "in-plane" fibers is particularly damaging to the accuracy of fiber-orientation measurement, because the number of "in-plane" fibers is significantly smaller compared to fibers crossing the plane at greater angles. The Leeds system also tends to fit ellipses to clusters of fibers, rather than to separate fibers. This phenomenon was particularly pronounced for specimens with Ni-coated carbon fibers.

The fiber orientation obtained from the Leeds system was further scrutinized due to the reasons outlined above. Representative samples for glass-, carbon- and Ni-coated-carbon-filled materials were imaged at ORNL and analyzed at University of Illinois. Figure 5 shows comparison of Leeds and manual measurement for orientation tensor components for Ni-coated-fiber-filled specimen CS3I, which was expected to have large measurement errors. Only 1/6th of the sample was re-measured; however, good match between the data is already apparent. The same manual measurement on larger portions of AS3I and BF3D samples resulted in closer match of the Leeds results. Good match for all three specimens examined manually

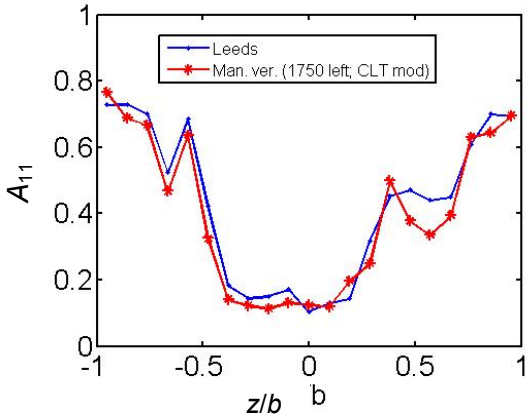

Figure 5. Comparison of Leeds and partial manual measurements for A_{11} (PNNLCS3I).

indicates that the Leeds system measures ellipse cross-sections with acceptable accuracy.

Preliminary burn-off tests revealed a wide range of fiber lengths present in molded samples. Standards and measurement techniques developed for short-fiber-reinforced plastics could not be used due to the wide range of fiber lengths and the tendency of the long fibers to bend. Procedures have been developed for fiber-length measurement of glass- and carbon-filled LFTs. The procedures consist of identical major steps; however, the execution of these steps differs due to different physical properties of glass and carbon fibers. These are the steps of fiber-length measurement:

1. composite coupon isolation
2. constrained removal of matrix material
3. fiber-sample isolation
4. filament dispersion
5. imaging and individual filament-length measurement

The size of a coupon cut out from a specimen must be large enough to prevent measurement of cut fibers. Materials examined in this project were molded with initial nominal fiber length of 12 mm, therefore, the distance of the center of the section - the location of interest - from any edge must be 12 mm or more.

The composite coupon is placed in an aluminum sheet-metal form whose inside dimensions correspond to the shape and area dimensions of the coupon. The sheet-metal form provides restraint at the edges of the coupon during the matrix-removal step, which was performed via burn-off. The form and its contents are sealed at the top and bottom with aluminum-foil lids. The form-height dimensions are greater than the coupon thickness to provide for some expansion of the fibers during matrix burn-off. This expansion is believed to facilitate the separation and spreading of the filaments during the dispersal step that follows later in this procedure.

The fiber-sample-isolation step involves isolating the central fibers of the residual fiber mass for subsequent collection and characterization. The process involves inserting the needle attached to a hypodermic syringe loaded with a liquid epoxy through the center of both the top and bottom lids of the aluminum form containing the fiber. The needle is withdrawn from the form and through the fiber stack while dispensing the epoxy through the needle at a constant rate. The continuous stream of epoxy results in approximately cylindrical column of resin that extends through the entire thickness of the fiber stack. The number of fibers collected from the specimen is proportional to the epoxy plug volume (diameter of the cylinder). Factors that control the volume include the resin's viscosity, the needle gage and the withdrawal rate of the needle through the fiber stack. The resin injection is conducted with the aid of an actuator for better control of uniform epoxy deposition. After injection, the epoxy is allowed to gel at room temperature and the resin is subsequently cured. Filaments in the vicinity of the epoxy are thereby bonded in-situ to the epoxy cylinder. The bonded fibers are extracted by removing the fiber stack with epoxy plug from the aluminum form, manually shaking the specimen and short blasts of low-pressure air. Figure 6 is a photograph of an extracted carbon fiber-and-epoxy plug specimen. Long and shorter fibers are visibly attached to the plug specimen along its length.

Figure 6. Extracted carbon fiber-and-epoxy plug specimen.

A major portion of development effort was devoted to the technique of long-carbon-fiber separation. Long carbon fibers exhibit the tendency to form filament clumps, therefore preventing measurement of individual filament length. A number of unsuccessful trials involving liquids and various chemicals did not result in an acceptable technique. Mechanical methods usually caused breakage of the filaments.

The newly developed dispersal process relies on a corona field provided from a high-frequency generator to create fields of static charge in the vicinity of the carbon filaments and a substrate surface. In this case, the substrate is a ply of paper supported on a notebook pad of paper that is approximately 6-mm thick. The paper stack is elevated by supports so that the corona field from the tip of the high-frequency generator can be applied from beneath. A portion of the residual fiber clumps are placed on the paper and the high-frequency generator is switched on to generate the corona field beneath the paper stack As the paper and carbon filaments acquire static charge, two phenomena occur that aid in separation and dispersal of the carbon filaments. One is that the carbon filaments seem to repel each other and, when the residual fiber mass is sufficiently small, fly apart and disperse. The other is that the carbon fibers are attracted to the charged substrate and tend to adhere to the paper so long as the corona field is applied. The procedure for dispersal therefore involves gently moving the residual fiber clumps across the paper surface while generating the statically-charged fields in their vicinity with the high-frequency generator. The carbon filaments from the clumped fiber mass gradually are "shed" from the outside of the clump and onto the paper. This shedding process occurs with the smallest filaments first, leaving the longer filaments to be dispersed later in the process. Manipulation of the clumps is done manually. Wooden sticks from cotton swabs work well for this purpose as well as insulating the operator from electrical shocks.

As-is, the carbon-fiber-dispersal technique is rudimentary, but effective. A little art and technique on the part of the operator is required to effectively disperse all of the fiber clumps and, depending on circumstances (clump size, fiber length distribution, etc.), some strategies work better than others. Some care is required to avoid breaking the filaments during manipulation. Applying the corona field directly to the carbon fibers themselves will induce arcing that is definitely damaging to the fibers. The technique becomes less effective as the paper substrate becomes loaded with dispersed filaments, so changing the paper at regular intervals is recommended.

Following dispersal, a layer of clear adhesive-backed laminating film is applied over the dispersed carbon filaments and the copier printer paper substrate. The laminating film fixes the fibers in place to the paper so they cannot shift, re-combine, fly away, etc. These laminated sheets can then be transported, stored for future reference, etc. Digital images of the carbon filaments are scanned through the clear laminating film and into a computer file for later analysis.

The ease of glass-fiber dispersion depends on proper amount of expansion during the first constrained burn-off. Complete constraint results in an entangled mass of fibers of approximately original sample thickness because glass fibers anneal at burn-off temperatures. Attempting to separate fibers from this entangled state is impractical. Constraint-free burn-off would result in dislocation of fibers, thereby preventing subsequent isolation of a representative sample. Identical steps for fiber-sample separation can be followed. Dispersion of glass fibers is performed on glass Petri dishes by gently tapping the dish. The fibers exhibit affinity for the glass surface. As in the case of carbon-fiber separation, the short fibers adhere to the surface first. Petri dishes with dispersed glass fibers can be scanned using a regular scanner. Traditionally, multiple images were collected from a microscope with an x-y stage and then joined. The use of a scanner considerably simplifies and shortens the measurement process. It is also possible to consider the use of automated image-analysis software for fiber-length evaluation, as problems with imperfectly-joined images are eliminated.

Fiber-length distribution is currently determined by manually measuring the fiber length of fibers using the Image J software. Presently-available automated software packages can not cope with typical LFT bent fibers and multiple fiber ends in the same location. A prototype software package capable of length measurement of approximately straight fibers and identification and isolation of problematic measurements is under development.

Mechanical tests were performed on all specimen geometries and materials. Elastic properties corresponding to certain locations considered for fiber-orientation and fiber-length measurements were obtained. Carbon-fiber-filled specimens did not

perform as expected and poor fiber-matrix interface is suspected based on scanning electron microscope images showing no resin residue present on carbon fibers after fracture. Preliminary measurements of the coefficient of thermal expansion were performed. Processes active within the material at elevated temperatures resulted in highly non-linear thermal expansion. Therefore, the results of these measurements are not conclusive at this time.

Three students from Virginia Polytechnic Institute, University of Illinois and University of Tennessee actively participated in developing experimental techniques and performing measurements while working at ORNL.

Computation of LFT Thermoelastic Properties

Computation of LFT elastic properties: The measurement of fiber lengths in LFT samples shows that the actual fiber-length distributions (FLDs) are unsymmetrical and exhibit a shape having a sharp peak in the short fiber range and a long "tail" towards the long fiber range (> 1mm). The Weibull's distribution that contains two shape parameters named "*b*" and "*c*" can be used to represent such a distribution. The Weibull's probability distribution function is given by:

$$f(l) = \frac{c}{b}\left(\frac{l}{b}\right)^{c-1} e^{-\left(\frac{l}{b}\right)^{c}} \qquad (7)$$

where *l* is the fiber length. The stiffness matrix of a unidirectional (UD) fiber composite containing a fiber length distribution (e.g. represented by Eq. (7)) is then computed as:

$$C_{ijkl} = \frac{\int_0^\infty C^*_{ijkl}(l/d) f(l)\, dl}{\int_0^\infty f(l) dl} \qquad (8)$$

where $C^*_{ijkl}(l/d)$ is the stiffness matrix of the UD fiber composite having the aspect ratio *l/d*. In this work, the Eshelby-Mori-Tanaka method [13-14] was applied to compute $C^*_{ijkl}(l/d)$, and after the calculation of C_{ijkl} using Eq. (8), the elastic stiffness of the actual composite in which the fiber orientation was achieved after injection molding was computed using the orientation averaging method [10]:

$$\begin{aligned}\overline{C}_{ijkl} &= B_1\, A_{ijkl} + B_2(A_{ij}\delta_{kl} + A_{kl}\delta_{ij}) + \\ &B_3(A_{ik}\delta_{jl} + A_{il}\delta_{jk} + A_{jl}\delta_{ik} + A_{jk}\delta_{il}) \\ &+ B_4\delta_{ij}\delta_{kl} + B_5(\delta_{ik}\delta_{jl} + \delta_{il}\delta_{jk})\end{aligned} \qquad (9)$$

where the coefficients B_i (i = 1, 5) are related to the stiffness components of the UD transversely isotropic composite (Eq. (8)). The results are illustrated for the moduli E_{11}, E_{22} and E_{33} in Figures 7(a-c) for the PNNLAF3D material (location B), respectively. On these figures are presented the results obtained using one and two Weibull's FLDs, and also those obtained using the average fiber length (1.42 mm). The results based on one Weibull's FLD are very close to the values based on the use of two Weibull's distributions. This shows that it is not necessary to closely capture the experimental distribution with two Weibull's fits, and the results based on the average fiber length constitute a fair approximation of the values obtained by the use of one or two Weibull's FLDs.

Computation of thermal expansion coefficients: The Eshelby-Mori-Tanaka approach to predict the elastic properties of fiber composites can be extended to compute the thermal expansion coefficients (CTEs) of these materials. The key idea is to incorporate the thermal strain in the governing equations to first obtain the CTEs for the UD fiber composite [15]:

$$\boldsymbol{\alpha}_c = \boldsymbol{\alpha}_m + \frac{f\,(\boldsymbol{\varepsilon}^* + \boldsymbol{\alpha}^*)}{\Delta T} \qquad (10)$$

where *f* is the fiber volume fraction, ΔT is the temperature change; $\boldsymbol{\alpha}_c$ and $\boldsymbol{\alpha}_m$ are the CTEs of the UD fiber composite and matrix material, respectively. $\boldsymbol{\varepsilon}^*$ is defined as the eigenstrain and $\boldsymbol{\alpha}^*$ is the strain resulting from the mismatch of CTEs of the constituents. Next, the CTE solution $\overline{\alpha}_{ij}$ for the actual random fiber composite is determined from the CTEs and stiffness of the UD fiber composite, the second and fourth-order orientation tensors using the *aggregate averaging method* [16]:

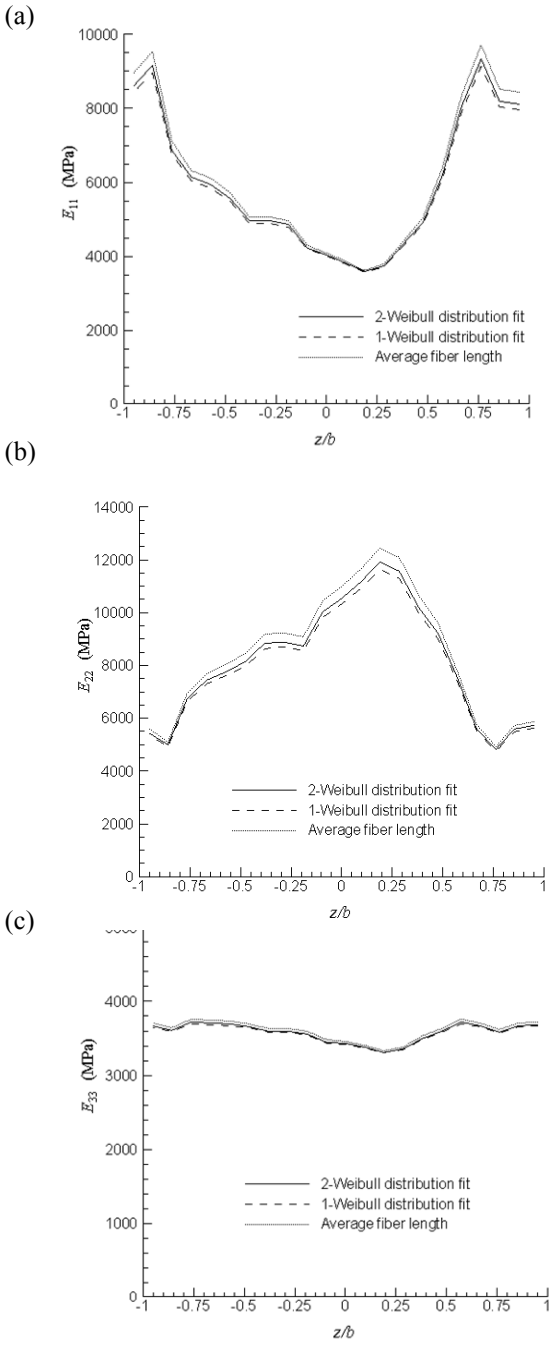

Figure 7. Moduli (a) E_{11}, (b) E_{22}, and (c) E_{33} predicted along the specimen thickness direction (PNNLAF3D, location B).

$$\overline{\alpha}_{ij} = \overline{C}^{-1}_{ijkl}\hat{\alpha}_{kl}$$
$$\hat{\alpha}_{ij} = \left\langle C_{ijkl}\alpha^{c}_{kl} \right\rangle = \hat{\alpha}_1 A_{ij} + \hat{\alpha}_2 \delta_{ij} \quad (11)$$

where $\hat{\alpha}_1$ and $\hat{\alpha}_2$ are related to the CTEs of the UD fiber composite. The model to compute CTEs of LFTs has been implemented in the homogenization procedure using the Eshelby-Mori-Tanaka framework. Results will be presented in the next report.

Conclusions

During this year our efforts were focused on the technical assessment of current process models, computational capabilities, and experimental methods that enable us to address the issues arising in LFTs. The feasibility assessment phase has been successfully completed. In addition, computational models and tools have also been developed to predict the thermoelastic properties of LFTs. These models account for fiber orientation and length distributions. The following conclusions have been drawn:

- LFT microstructure possesses a skin/shell/core layered structure as observed in SFTs. However, flow-direction alignment in the shell layers is significantly lower in the LFT samples than in SFTs.
- In addition to the fiber orientation, there are emerging variables for LFTs which are fiber length distribution, fiber volume fraction, fiber curvature, and orientation clustering.
- The current fiber orientation and constitutive models can adequately predict the fiber orientation, suspension viscosity in dilute and semi-concentrated regimes. However, these models have limitations to capture the fiber orientation in concentrated regimes. This is true for both short- or long-fiber systems.
- The Hele-Shaw assumption for flows in thin cavities applies to both short- and long-fiber systems.
- The best fits of the RSC model to LFT fiber orientation data show that the SRF value for carbon fibers is higher than the SRF value for glass fibers. This suggests that fiber stiffness plays a role in determining SRF.

- Neither the standard fiber orientation model nor the new RSC model can predict fiber orientation in LFT samples to the level of accuracy needed for predictive engineering.
- The fundamental limitation of the fiber orientation model seems to reside in the interaction term. This term needs to be improved to account for the rotation of long fibers and the anisotropic character of the fiber-fiber interaction which cannot be adequately represented by an isotropic rotary diffusion term.
- The data for Ni-coated carbon fiber is more erratic than for uncoated carbon fiber. Thus, we have not established that Ni-coated carbon fiber is a direct substitute for uncoated carbon fiber in terms of fiber orientation behavior.
- The Leeds system provides accurate measurement of fiber cross-sections.
- Long carbon fibers can be separated using corona field of static electricity.
- Validation of the thermoelastic property prediction tool will be achieved by comparing the predicted moduli with the corresponding experimental values.

References

1. B.N. Nguyen, J.D. Holbery, V. Kunc (2006). "Property Prediction Tools for Tailored Polymer Composite Structures." FY06 semi annual report.

2. B.N. Nguyen, J.D. Holbery, M.T. Smith, V. Kunc, R.E. Norris, J. Phelps, C.L. Tucker III (2006). "Assessment of Current Process Modeling Approaches to Determine Their Limitations, Applicability and Developments Needed for Long-Fiber Thermoplastic Injection-Molded Composites." PNNL internal report No. PNNL-16236.

3. C.L. Tucker III and S.G. Advani (1994). "Processing of Short-Fiber Systems." In: Flow and Rheology in Polymer Composites Manufacturing, S.G. Advani, Ed., Elsevier Science, 147-202.

4. M. Rahnama, D.L. Koch, and E.S.G. Shaqfeh (1995). "The Effect of Hydrodynamic Interactions on the Orientation Distribution in a Fiber Suspension Subject to Simple Shear Flow." *Phys. Fluids*, 7(3): 487-506.

5. C. Servais, J.-A.E. Manson, and S. Toll (1999). "Fiber-Fiber Interaction in Concentrated Suspensions : Disperse Fibers." *J. Rheol.*, 43(4), 991-997.

6. M. Djalili-Moghaddam and S. Toll (2005). "A Model for Short-Range Interactions in Fiber Suspensions." *J. Non-Newtonian Fluid Mech.*, 132: 73-83.

7. F. Folgar and C.L. Tucker III (1984). "Orientation Behavior of Fibers in Concentrated Suspensions." *J. Reinf. Plast. Comp.*, 3:98-119.

8. S.G. Advani and C.L. Tucker III (1987). "The Use of Tensors to Describe and Predict Fiber Orientation in Short-Fiber Composites." *J. Rheol.*, 31 (8):751-784.

9. H.M. Huynh (1999). Improved fiber orientation predictions for injection-molded composites. Master's thesis, University of Illinois, Urbana, IL.

10. J.H. Phelps and C.L. Tucker III (2006). "Assessing Fiber Orientation Prediction Capability for Long-Fiber Thermoplastic Composites." Technical Report submitted to PNNL, University of Illinois at Urbana-Champaign.

11. R.S. Bay and C.L. Tucker III (1992). "Fiber Orientation in Simple Injection Moldings. Part I: Theory and Numerical Methods. *Polym. Compos.*, 13:317-331.

12. P.J. Hine, N. Davidson, R.A. Duckett, A.R. Clarke, I.M. Ward (1996). "Hydrostatically Extruded Glass-Fiber-Reinforced Polyoxymethylene. I: The development of Fiber and Matrix Orientation." *Polym. Compo.*, 17:720-729.

13. J.D. Eshelby (1957). "The determination of The Elastic Field of An Ellipsoidal Inclusion and Related Problems." *Proc. Royal Soc. London*, A 241:376-396.

14. T. Mori, K. Tanaka (1973). "Average Stress in Matrix and Average Elastic Energy of Materials with Misfitting Inclusions." *Acta Metall.*, 21:571-574.

15. Y. Takao Y, M. Taya M (1985). "Thermal Expansion Coefficients and Thermal Stresses in an Aligned Short Fiber Composite with Application to A Short Carbon Fiber/Aluminum." *J. Applied Mechanics*, 52:806-810.

16. C. Camacho, C.L. Tucker III, S. Yalvac, R.L. McGee (1990). "Stiffness and Thermal Expansion Predictions for Hybrid Short-Fiber Composites". *Polym. Compos.*, 11:229-239.

Presentations and Publications

Experimental Methods to Evaluate Fiber Length and Orientation Distribution of Long Glass Fibers in Injection Molded Thermoplastics, Gregorio Velez-Garcia, Vlastimil Kunc, Fiber Society Conference, October 10-12, 2005, Knoxville, TN.